nodule (true-positive detection) was measured by a different radiologist (M.K.) using digital calipers.

Radiation Dose Evaluation

To evaluate the radiation dose, the estimated CT dose index volume (CTDIvol) and dose-length product (DLP) were recorded for each image data set after the completion of the CT examination, according to the dose report. Effective doses were estimated from DLP using a constant of 0.014 mSv/mGy-cm, as reported in the literature for chest CT.[33]

Statistical Analyses

The results of each radiologist in the ultralow-dose MBIR and the low-dose ASIR were compared with the reference standard, and the sensitivity in detecting pulmonary nodules was assessed. The statistical significance of any difference between the ultralow-dose MBIR and the low-dose ASIR for each radiologist was assessed using the McNemar test. The data were analyzed using JMP 9.0.0 software (SAS Institute, Cary, NC). The results, including confidence levels, were used to generate jackknife alternative free-response receiver operating characteristic (JAFROC) plots. The JAFROC analysis[34,35] was used for the evaluation of radiologist performance in the detection of pulmonary nodules in the ultralow-dose MBIR and the low-dose ASIR. The JAFROC analysis has been proposed for estimating the statistical significance of differences between modalities when location issues are relevant and has been widely used in multiple previous studies in the radiology literature.[36–39] The JAFROC analysis is based on a FROC paradigm and accounts for reader variation.[34,35,40] Conventional ROC analysis is of limited value for this kind of application because only 1 response per image can be used per case, and the location of the response cannot be taken into account in the evaluation. In contrast, the FROC analysis allows evaluation of the performance of radiologists in diagnosing medical images using multiple responses, each with information on the confidence level and location. For statistical testing of differences in radiologist performance between the ultralow-dose MBIR and the low-dose ASIR, JAFROC version 4.0 software (http://www.devchakraborty.com) was applied to estimate figure-of-merit (FOM) values (*analog of the area under the ROC curve*, defined as the probability that a true-positive confidence rating exceeds any false-positive rating on cases without nodules) of each modality (the ultralow-dose MBIR and the low-dose ASIR) with 95% confidence intervals. An F test was used internally for the analysis of variance, yielding a P value for rejecting the null hypothesis of no difference between the 2 modalities. A value of $P < 0.05$ was considered statistically significant.

RESULTS

Radiation Dose

Radiation dose descriptors acquired with the reference-, low-, and ultralow-dose CT for the 59 patients are summarized in Table 2. Compared with the low-dose CT, a 78.1% decrease in DLP was seen with the ultralow-dose CT.

TABLE 2. Comparison of Radiation Dose for the Reference-, Low-, and Ultralow-Dose CT

	Reference-Dose	Low-Dose	Ultralow-Dose
CTDIvol, mGy	8.29 (4.60)	1.77 (1.29)	0.39 (0.00)
DLP, mGy-cm	307.7 (178.1)	66.0 (50.8)	14.5 (1.1)
ED, mSv	4.31	0.92	0.20

Data represent mean (SD) for each value.

Compared with the low-dose CT, a 78.0% decrease in CTDIvol and a 78.1% decrease in DLP were seen with the ultralow-dose CT.

TABLE 3. Number and Size of Nodules

Pattern of Nodule	Number	Size, mm
GGO	18	8.0 (4.4)
Partly solid	11	11.3 (6.4)
Solid	55	7.0 (4.6)

Data represent mean (SD) for each value.

Results of Nodule Detection

The consensus panel found 84 noncalcified nodules of 4 mm in diameter or more on the reference-dose ASIR (GGO, n = 18; partly solid, n = 11; solid, n = 55) in the 59 patients. No nodules were found in 18 patients. The mean diameter of each nodule according to the 3 radiological patterns is shown in Table 3.

Sensitivity data for the detection of overall nodules and according to the 3 radiological patterns are shown in Table 4. No significant differences were identified between the low-dose ASIR and the ultralow-dose MBIR of both radiologists for the overall nodule detection (61%–67%; $P = 0.48$–0.69). Similarly, no significant differences were observed for GGO, partly solid, or solid nodule detection (50%–91%; $P = 0.08$–0.65).

Jackknife Alternative Free-Response Receiver Operating Characteristic Analysis

Figure-of-merit values for the 2 radiologists in the detection of all pulmonary nodules are summarized in Table 5. In the overall nodules, no significant differences were identified between the low-dose ASIR and the ultralow-dose MBIR in the FOM values ($P = 0.57$). The JAFROC analysis also revealed no significant differences between the low-dose ASIR and the ultralow-dose MBIR for GGO, partly solid, or solid nodule detection ($P = 0.21$–0.90).

DISCUSSION

In the present study, nodule detectability in the low-dose chest CT reconstructed with ASIR and the ultralow-dose CT reconstructed with MBIR were directly compared in the same patients. Diagnostic performance for nodule detection in the MBIR images acquired with nearly 80% dose reduction (ultralow-dose) did not differ significantly from that in the low-dose ASIR (representing the dose for lung cancer screening CT), irrespective of the characteristics of the nodules as GGO, partly solid, or solid. To the best of our knowledge, this is the first clinical study to evaluate the ability of MBIR to allow further radiation dose reduction over ASIR by directly comparing the diagnostic performance for the detection of pulmonary nodules in the same patients.

As radiation dose decreases by 1/x, the image noise is known to increase by the square root of x in FBP and subsequently in hybrid IR algorithms that involve blending with FBP such as ASIR, which renders the visualization of nodules in dose-reduced chest CT. However, our preliminary results from phantom experiments indicated that MBIR, a pure IR algorithm, behaves differently: as radiation dose decreases by 1/x, image noise increases only by the fourth root of x (unpublished data), resulting in a relatively lower increase in noise compared with FBP or hybrid IR-reconstructed images. Moreover, MBIR also provides significant reductions in streak artifacts and significant improvements in spatial resolution.[25,26] The ultralow-dose MBIR in the present study showed no significant differences in the overall nodule detection from the low-dose ASIR in sensitivity for both radiologists. Our sensitivity data (50%–91%) are similar to those in a previous study that assessed pulmonary nodule detection in standard-dose CT.[39] The JAFROC analysis also revealed no significant differences between the low-dose ASIR and the ultralow-dose MBIR, irrespective of nodule characteristics as GGO, partly solid, or solid

TABLE 4. Sensitivity Data for Nodule Detection

Pattern of Nodule	Radiologist 1			Radiologist 2		
	Ultralow MBIR	Low ASIR	*P*	Ultralow MBIR	Low ASIR	*P*
Overall (n = 84)	56/84 (67)	54/84 (64)	0.69	55/84 (65)	51/84 (61)	0.48
GGO (n = 18)	12/18 (67)	9/18 (50)	0.08	9/18 (50)	11/18 (61)	0.41
Partly solid (n = 11)	10/11 (91)	7/11 (64)	0.08	7/11 (64)	6/11 (55)	0.65
Solid (n = 55)	34/55 (62)	38/55 (69)	0.37	39/55 (71)	34/55 (62)	0.28

No significant differences were seen between the low-dose ASIR and the ultralow-dose MBIR for both radiologists for the overall nodule, GGO, partly solid, or solid nodule detection (McNemar test).

nodules. A pixelated blotchy appearance was noted in almost all ultralow-dose MBIR images but did not seem to affect the diagnostic performance of the radiologists, neither of whom had little experience with MBIR images before the present study. Recently, Yamada et al[41] compared the diagnostic performance of "ultralow-dose" MBIR (ED, 0.17 mSv) and "ultralow-dose" FBP for pulmonary nodule detection, using "low-dose" FBP (ED, 2.10 mSv) as the reference standard. The present study differs from their study in that we used reference-dose ASIR to establish a more robust reference standard, and moreover, we directly compared the diagnostic performance of the ultralow-dose MBIR and the low-dose ASIR to evaluate whether MBIR enables further radiation dose reduction over ASIR. The present results indicate the substantial potential of MBIR for achieving further radiation dose reductions without affecting nodule detectability, irrespective of nodule characteristics. The results also indicate that ultralow-dose CT may become feasible with the use of a pure IR algorithm such as MBIR.

Many studies have examined the use of low-dose chest CT for lung cancer screening.[6–9,42–45] The radiation dose delivered by lung screening CT has been aimed to be as low as technologically possible, typically ranging from 0.6 to 1.5 mSv in previous lung cancer screening CT trials.[7–9] The ED for the low-dose CT in the present study turned out to be lower than the average ED is for the low-dose CT described in the NLST (1.5 mSv),[9] most likely because of the small body size of the patients. The ultralow-dose CT was acquired with a nearly 80% reduction in dose compared with the low-dose CT. The present results indicate that lung cancer screening CT may be lowered even to ultralow-dose levels using pure IR algorithms such as MBIR. We acknowledge that the patients in the present study do not necessarily reflect the target population for lung cancer screening in terms of clinical and social characteristics, prevalence of lesions, or background lung conditions. However, our results strongly support the potential of ultralow-dose MBIR for the purpose of lung cancer screening. Longitudinal studies with an increased number of participants (the sample size should be determined by statistical power analysis) in a targeted population specifically aimed at assessing lung cancer mortality are necessary. Ultralow-dose MBIR should also be assessed in future studies for other screening purposes, such as CT colonography. In addition, MBIR may be considered for patients who require substantial dose reduction, such as infants and young patients, and those with radiosensitive genetic disorders such as ataxia telangiectasia. Because the impact of MBIR on lesion detectability may differ between body regions and for different lesion characteristics (eg, size, attenuation, contrast), MBIR should be evaluated according to the purpose of each examination in future studies.

Several limitations of this study must be considered. First, the body size of patients in this study was generally small. Our results of the ultralow-dose CT acquired using a fixed tube current-time product of 5 mA s may not necessarily apply to patients who are extremely large or obese. This needs to be investigated in future studies using automatic tube current modulation with appropriate NI settings. Second, all chest CT examinations were performed without intravenous administration of contrast medium. The contrast enhancement effect itself has not yet been thoroughly assessed in MBIR, and the presence of streak artifacts from the superior vena cava is another important issue that needs to be considered in contrast-enhanced chest CT. These are not issues in lung cancer screening CT, which does not usually involve the use of contrast medium, but these issues should be investigated in future studies to further assess the feasibility of MBIR for clinical use. A third limitation of the study is that the results may not be applicable to similar iterative reconstruction methods available from other vendors.

In conclusion, MBIR enables a nearly 80% reduction in radiation dose for chest CT from a low-dose level to an ultralow-dose level, without affecting nodule detectability. Ultralow-dose CT is expected to become feasible for lung cancer screening with the use of pure IR algorithms such as MBIR.

TABLE 5. Figure-of-Merit Values Obtained From the JAFROC Analysis

Pattern of Nodule	FOM Values (95% Confidence Interval)		
	Ultralow MBIR	Low ASIR	*P*
Overall (n = 84)	0.817 (0.776–0.859)	0.802 (0.746–0.857)	0.57
GGO (n = 18)	0.793 (0.708–0.879)	0.750 (0.654–0.846)	0.22
Partly solid (n = 11)	0.885 (0.511–1.260)	0.794 (0.659–0.928)	0.21
Solid (n = 55)	0.832 (0.735–0.929)	0.827 (0.742–0.913)	0.90

No significant differences in JAFROC FOM values were identified between the low-dose ASIR and the ultralow-dose MBIR for the overall nodule, GGO, partly solid, or solid nodule detection.

ACKNOWLEDGMENTS

The authors thank Kosuke Sasaki, MS, and Koji Segawa, RT, for their technical support and assistance in data acquisition.

REFERENCES

1. Ferlay J, Shin H, Bray F, et al. Estimates of worldwide burden of cancer in 2008: GLOBOCAN 2008. *Int J Cancer*. 2010;127:2893–2917.
2. Cancer Facts & Figures 2012. American Cancer Society Web site. http://www.cancer.org/Research/CancerFactsFigures/CancerFactsFigures/cancer-facts-figures-2012. Accessed 30 September 2012.
3. Cerfolio RJ, Bryant AS. Survival of patients with true pathologic stage I non-small cell lung cancer. *Ann Thorac Surg*. 2009;88:917–923.
4. Carr SR, Schuchert MJ, Pennathur A, et al. Impact of tumor size on outcomes after anatomic lung resection for stage 1A non-small cell lung cancer based on the current staging system. *J Thorac Cardiovasc Surg*. 2012;143:390–397.
5. National Lung Screening Trial Research Team, Aberle DR, Adams AM, et al. Reduced lung-cancer mortality with low-dose computed tomographic screening. *N Engl J Med*. 2011;365:395–409.
6. Henschke CI, McCauley DI, Yankelevitz DF, et al. Early lung cancer action project: a summary of the findings on baseline screening. *Oncologist*. 2001; 6:147–152.

7. Swensen SJ, Jett JR, Hartman TE, et al. Lung cancer screening with CT: Mayo Clinic experience. *Radiology.* 2003;226:756–761.
8. Diederich S, Thomas M, Semik M, et al. Screening for early lung cancer with low-dose spiral computed tomography: results of annual follow-up examinations in asymptomatic smokers. *Eur Radiol.* 2004;14:691–702.
9. National Lung Screening Trial Research Team, Aberle DR, Berg CD, et al. The National Lung Screening Trial: overview and study design. *Radiology.* 2011;258:243–253.
10. Kalra MK, Maher MM, Toth TL, et al. Strategies for CT radiation dose optimization. *Radiology.* 2004;230:619–628.
11. Heyer CM, Mohr PS, Lemburg SP, et al. Image quality and radiation exposure at pulmonary CT angiography with 100- or 120-kVp protocol: prospective randomized study. *Radiology.* 2007;245:577–583.
12. Baumueller S, Alkadhi H, Stolzmann P, et al. Computed tomography of the lung in the high-pitch mode: is breath holding still required? *Invest Radiol.* 2011;46:240–245.
13. Kalra MK, Maher MM, Sahani DV, et al. Low-dose CT of the abdomen: evaluation of image improvement with use of noise reduction filters pilot study. *Radiology.* 2003;228:251–256.
14. Prakash P, Kalra MK, Digumarthy SR, et al. Radiation dose reduction with chest computed tomography using adaptive statistical iterative reconstruction technique: initial experience. *J Comput Assist Tomogr.* 2010;34:40–45.
15. Leipsic J, Labounty TM, Heilbron B, et al. Adaptive statistical iterative reconstruction: assessment of image noise and image quality in coronary CT angiography. *AJR Am J Roentgenol.* 2010;195:649–654.
16. Singh S, Kalra MK, Hsieh J, et al. Abdominal CT: comparison of adaptive statistical iterative and filtered back projection reconstruction techniques. *Radiology.* 2010;257:373–383.
17. Prakash P, Kalra MK, Kambadakone AK, et al. Reducing abdominal CT radiation dose with adaptive statistical iterative reconstruction technique. *Invest Radiol.* 2010;45:202–210.
18. Singh S, Kalra MK, Gilman MD, et al. Adaptive statistical iterative reconstruction technique for radiation dose reduction in chest CT: a pilot study. *Radiology.* 2011;259:565–573.
19. Kilic K, Erbas G, Guryildirim M, et al. Lowering the dose in head CT using adaptive statistical iterative reconstruction. *AJNR Am J Neuroradiol.* 2011; 32:1578–1582.
20. Mieville FA, Gudinchet F, Rizzo E, et al. Paediatric cardiac CT examinations: impact of the iterative reconstruction method ASIR on image quality—preliminary findings. *Pediatr Radiol.* 2011;41:1154–1164.
21. Singh S, Kalra MK, Shenoy-Bhangle AS, et al. Radiation dose reduction with hybrid iterative reconstruction for pediatric CT. *Radiology.* 2012;263:537–546.
22. Craig O, O'Neill S, O'Neill F, et al. Diagnostic accuracy of computed tomography using lower doses of radiation for patients with Crohn's disease. *Clin Gastroenterol Hepatol.* 2012;10:886–892.
23. Desai GS, Uppot RN, Yu EW, et al. Impact of iterative reconstruction on image quality and radiation dose in multidetector CT of large body size adults. *Eur Radiol.* 2012;22:1631–1640.
24. Kaza RK, Platt JF, Al-Hawary MM, et al. CT enterography at 80 kVp with adaptive statistical iterative reconstruction versus at 120 kVp with standard reconstruction: image quality, diagnostic adequacy, and dose reduction. *AJR Am J Roentgenol.* 2012;198:1084–1092.
25. Thibault JB, Sauer KD, Bouman CA, et al. A three-dimensional statistical approach to improved image quality for multislice helical CT. *Med Phys.* 2007;34:4526–4544.
26. Yu Z, Thibault JB, Bouman CA, et al. Fast model-based x-ray CT reconstruction using spatially nonhomogeneous ICD optimization. *IEEE Trans Image Process.* 2011;20:161–175.
27. Nelson RC, Feuerlein S, Boll DT. New iterative reconstruction techniques for cardiovascular computed tomography: how do they work, and what are the advantages and disadvantages? *J Cardiovasc Comput Tomogr.* 2011;5:286–292.
28. Katsura M, Matsuda I, Akahane M, et al. Model-based iterative reconstruction technique for radiation dose reduction in chest CT: comparison with the adaptive statistical iterative reconstruction technique. *Eur Radiol.* 2012;22:1613–1623.
29. Singh S, Kalra MK, Do S, et al. Comparison of hybrid and pure iterative reconstruction techniques with conventional filtered back projection: dose reduction potential in the abdomen. *J Comput Assist Tomogr.* 2012;36:347–353.
30. Strub WM, Weiss KL, Sun D. Hybrid reconstruction kernel: optimized chest CT. *AJR Am J Roentgenol.* 2007;189:W115–W116.
31. Weiss KL, Cornelius RS, Greeley AL, et al. Hybrid convolution kernel: optimized CT of the head, neck, and spine. *AJR Am J Roentgenol.* 2011;196:403–406.
32. Prakash P, Kalra MK, Ackman JB, et al. Diffuse lung disease: CT of the chest with adaptive statistical iterative reconstruction technique. *Radiology.* 2010; 256:261–269.
33. American Association of Physicists in Medicine. The measurement, reporting, and management of radiation dose in CT; January 2008. Available at: http://www.aapm.org/pubs/reports/rpt_96.pdf. Accessed September 30, 2012.
34. Chakraborty DP, Berbaum KS. Observer studies involving detection and localization: modeling, analysis, and validation. *Med Phys.* 2004;31:2313–2330.
35. Chakraborty DP. Analysis of location specific observer performance data: validated extensions of the jackknife free-response (JAFROC) method. *Acad Radiol.* 2006;13:1187–1193.
36. Vikgren J, Zachrisson S, Svalkvist A, et al. Comparison of chest tomosynthesis and chest radiography for detection of pulmonary nodules: human observer study of clinical cases. *Radiology.* 2008;249:1034–1041.
37. Hirose T, Nitta N, Shiraishi J, et al. Evaluation of computer-aided diagnosis (CAD) software for the detection of lung nodules on multidetector row computed tomography (MDCT): JAFROC study for the improvement in radiologists' diagnostic accuracy. *Acad Radiol.* 2008;15:1505–1512.
38. Zachrisson S, Vikgren J, Svalkvist A, et al. Effect of clinical experience of chest tomosynthesis on detection of pulmonary nodules. *Acta Radiol.* 2009;50:884–891.
39. Yanagawa M, Honda O, Yoshida S, et al. Commercially available computer-aided detection system for pulmonary nodules on thin-section images using 64 detectors-row CT: preliminary study of 48 cases. *Acad Radiol.* 2009;16:924–933.
40. Chakraborty DP. Maximum likelihood analysis of free-response receiver operating characteristic (FROC) data. *Med Phys.* 1989;16:561–568.
41. Yamada Y, Jinzaki M, Tanami Y, et al. Model-based iterative reconstruction technique for ultralow-dose computed tomography of the lung: a pilot study. *Invest Radiol.* 2012;47:482–489.
42. Sone S, Li F, Yang ZG, et al. Results of three-year mass screening programme for lung cancer using mobile low-dose spiral computed tomography scanner. *Br J Cancer.* 2001;84:25–32.
43. Nawa T, Nakagawa T, Kusano S, et al. Lung cancer screening using low-dose spiral CT: results of baseline and 1-year follow-up studies. *Chest.* 2002; 122:15–20.
44. Sobue T, Moriyama N, Kaneko M, et al. Screening for lung cancer with low-dose helical computed tomography: anti-lung cancer association project. *J Clin Oncol.* 2002;20:911–920.
45. Gohagan JK, Marcus PM, Fagerstrom RM, et al. Final results of the Lung Screening Study, a randomized feasibility study of spiral CT versus chest x-ray screening for lung cancer. *Lung Cancer.* 2005;47:9–15.

APPENDIX

Adaptive iterative reconstruction and MBIR are new IR algorithms. Unlike the conventional FBP, which is based on simpler mathematical assumptions of the tomographic imaging system, IR generates a set of synthesized projections by accurately modeling the data collection process in CT. The model incorporates statistical system information (including photon statistics and electronic noise in the data acquisition system) and details of the system optics (including the size of each detector cell, dimensions of the focal spot, and the shape and size of each image voxel). The synthesized image is mathematically compared and corrected with the actual measurement to adjust estimation of the object's image. The technique then iterates this comparison and correction step to achieve close proximity between actual and measured projections. Inconsistencies in the projection measurement due to limited photon statistics and electronic noise are corrected with multiple iterations. These data-processing steps help to improve image quality from the noise and resolution perspectives but prolong the reconstruction duration compared with FBP because of the intensive computations particularly required for incorporating system optics information.

The ASIR technique models just the photons and electronic noise statistics that primarily affect image noise, which are not computationally intensive or time-consuming. This enables near real-time display of images at the time of imaging. Adaptive iterative reconstruction also differs from other IR techniques in that the vendor provides a blending tool to blend the FBP with the ASIR images ("hybrid IR"). This is accomplished by reconstruction of CT raw data with both FBP and ASIR techniques and then performing a weighted summation of each data set for the final reconstructed images. Prior studies have already shown that ASIR provides low-dose clinical images with a reduction in image noise compared with the FBP algorithm and preserved diagnostic value.[14–24]

The MBIR technique, on the other hand, is a pure IR technique that does not involve blending with FBP images and is mathematically more complex and accurate than ASIR is. Model-based iterative reconstruction not only incorporates modeling of photon and noise statistics such as ASIR but it also involves modeling of system optics. This is unlike ASIR, which uses an idealized set of system optics

(as does FBP), resulting in similar data use per image. Model-based iterative reconstruction analyzes the x-ray beam at the focal spot, then analyzes the x-ray beam as it passes through the patient's body, and, again, analyzes the x-ray beam as it strikes the detector. The algorithm weighs each data point so that noisy projections have less influence on the final results, and this allows more accurate image reconstruction. Phantom experiments have shown that MBIR has the potential to further reduce image noise, improve spatial resolution, and thereby allow further dose reduction without compromising image quality.[25,26] With the incorporation of system optics information and therefore a more accurate account of voxel and focal spot size and geometry, one can expect improvements in spatial resolution.[25,26] Because MBIR is a complicated algorithm, using multiple iterations and multiple models, the reconstruction time is significantly longer than FBP and the other IR techniques are, even with dedicated state-of-the-art parallel processors. The reconstruction time in the present study was approximately 1 hour per case, although the exact time was not recorded because it was not a feature of the application software.

Vol.2, No.4, 93-98 (2013)
http://dx.doi.org/10.4236/ojrm.2013.24013

Open Journal of Regenerative Medicine

Evaluation of *in vivo* migration of chondrocytes from tissue-engineered cartilage that was subcutaneously transplanted in mouse model

Mariko Matsuyama[1,2], Yuko Fujihara[2,3], Ryoko Inaki[1], Satoru Nishizawa[4], Satoru Nagata[5], Tsuyoshi Takato[1,3], Kazuto Hoshi[1,2,3*]

[1]Department of Sensory and Motor System Medicine, The University of Tokyo Hospital, Tokyo, Japan;
[*]Corresponding Author: pochi-tky@umin.net
[2]Department of Cartilage & Bone Regeneration (Fujisoft), Graduate School of Medicine, The University of Tokyo, Tokyo, Japan
[3]Division of Tissue Engineering, The University of Tokyo Hospital, Tokyo, Japan
[4]Translational Research Center, The University of Tokyo Hospital, Tokyo, Japan
[5]NAGATA Microtia and Reconstructive Plastic Surgery Clinic, Toda, Saitama, Japan

Received 20 August 2013; revised 20 September 2013; accepted 2 October 2013

ABSTRACT

For regenerative medicine, clarification of *in vivo* migration of transplanted cells is an important task to secure the safety of transplanted tissue. We had prepared tissue-engineered cartilage consisting of cultured chondrocytes with collagen hydrogel and a biodegradable porous polymer, and we clinically applied it for treatment of craniofacial anomaly. To verify the safety of this tissue-engineered cartilage, we had syngenically transplanted the tissue-engineered cartilage using chondrocytes harvested from EGFP-transgenic mice into subcutaneous pocket of wild type mice, and investigated localizations of transplanted chondrocytes in various organs including cerebrum, lung, liver, spleen, kidney, auricle, gastrocnemius, and femur. After 8 to 24 weeks of the transplantation, accumulation of cartilaginous matrices was observed in tissue-engineered cartilage, while EGFP-positive transplanted chondrocytes were localized in this area. Otherwise, no EGFP was immunohistochemically detected in each organ, suggesting that subcutaneously-transplanted chondrocytes do not migrate to other organs through the circulation. In cartilage tissue engineering using cultured chondrocytes, risk for migration and circulation of transplanted cells seemed negligible, and that ectopic growth of the cells was unlikely to occur, showing that this is safe technique with regard to the *in vivo* migration of transplanted cells.

Keywords: Cartilage; Tissue Engineering; Chondrocyte; Migration

1. INTRODUCTION

Autologous chondrocyte transplantation has been attracting attention as a treatment of defects and injuries of cartilage tissue, which has poor self-repairing capability [1]. Tissue-engineered cartilage with various properties, such as that prepared by injection of cultured chondrocyte suspension [1] and that gelled by mixing with hydrogel [2]. We developed tissue-engineered cartilage by adding autologous cultured chondrocytes to a porous scaffold made of a biodegradable polymer, poly-L-lactic acid (PLLA) [3], in which collagen hydrogel was used as a mucilage to retain cells within the scaffold [4]. Since this regenerative cartilage tissue has firm hardness and a 3D structure, it is applicable for patients with cartilage deformations and defects associated with craniofacial diseases and traumas. We are using this three-dimensionally tissue-engineered cartilage to treat nasal deformation in a congenital craniofacial anomaly, cleft lip and palate. Since this is a novel clinical technique, its safety should be fully investigated [3].

In the guidelines for safety of medical devices using cultured cells established by the Japanese government, the evaluation of *in vivo* migration of transplanted cells is included as a safety item. Since it has been reported that bone marrow mesenchymal stem cells, from which chondrocytes are originated, transfer into the circulation after

transplantation and engraft various organs other than bone marrow [5], the possibility for cultured chondrocytes to enter the circulation or to migrate to other organs cannot be ruled out. Thus, we performed this study to investigate the *in vivo* migration of cultured chondrocytes after transplantation, and to ensure its safety.

In our previous study, the tissue-engineered cartilage matured 8 weeks after transplantation [6]. At 8 weeks, the transplanted chondrocytes were completely embedded within cartilaginous matrices, which implied that migration of chondrocytes from the transplants to other organs hardly occurred after that time. Thus, we investigated whether transplanted auricular chondrocytes were migrated to other organs by 8 weeks after transplantation. In addition, we examined it also at 24 weeks to confirm long-term safety.

2. MATERIALS AND METHODS

Firstly, we collected auricular cartilage from the ears of EGFP-transgenic mice (6-week-old males, n = 3, Experimental Animal Division RIKEN BioResource Center, Ibaraki, Japan). After sacrifice by anesthesia with somnopentyl at a fatal dose, approximately 15-mm longitudinal incision was made in the parietal skin. The skin was entirely dissected from the incision line to the apex of the auricle. The auricular cartilage tissue was cut immediately before the tympanum and shaken in 0.15% collagenase solution at 37˚C for 8 hours [7]. The isolated auricular chondrocytes were seeded at 500,000 cells/well in a 6-well plastic plate and cultured in 2 mL of DMEM containing 5% fetal bovine serum, 5 μg/mL insulin, and 100 ng/mL fibroblast growth factor (FGF)-2 [8] as the primary culture. Approximately 1 × 108 cells were recovered after 2 passages (P2). These 1 × 108 cells and 1 mL of 1% collagen hydrogel (atelocollagen, Koken, Tokyo, Japan) were mixed on ice for about 10 minutes. The mixture was infiltrated into sterile PLLA porous scaffold (5 × 5 × 3 mm, KRI, Kyoto, Japan), and gelled in the dish at 37˚C for 2 hours to avoid drying (**Figure 1, 0 wk**).

The tissue-engineered cartilage composed of the PLLA/gel/cells (n = 3) was transplanted under the dorsal skin in C57BL/6 mice (Nippon Bio-Supp. Center, Tokyo, Japan) under anesthesia with 16 μL/animal of somnopentyl (**Figure 1, 0 wk**). The transplants and eight kinds of target organs (cerebrum, lung, liver, spleen, kidney, auricle, gastrocnemius, and femur) were excised after 8 and 24 weeks, fixed in 4% paraformaldehyde for one hour, immersed in PBS, and embedded in paraffin. The serial sections with a 5-μm thickness were then prepared.

After observation under excitation fluorescence, the sections of samples were subjected to toluidine blue staining, hematoxylin and eosin staining, and immunostaining of EGFP. To detect transplant-derived cells, non-serial 10 sections were selected from each organ [9], deparaffinize with xylene, hydrated with stepwise dilutions of ethanol, immersed in PBS, and subjected to immunostaining of EGFP. To activate antigen, the sections were placed in a mixture of 15 mL of Dako Real Target Retrieval Solution (×10) (Dako, Tokyo, Japan) and 135 mL of 98˚C hot water, boiled for 15 minutes, kept standing at room temperature for 15 minutes, and immersed in PBS for 5 minutes. This procedure was performed twice. For blocking, 10% normal goat serum was dripped on the sections and left standing at room temperature for 10 minutes. After removing moisture, the primary antibody, Invitrogen anti-green fluorescent protein rabbit IgG fraction (anti-GFP IgG) (Life Technologies Corporation, Carlsbad, CA, USA), was dripped on the sections (1:1000) and incubated at 37˚C for 90 minutes. For the control, normal rabbit IgG (SANTA CRUZ BIO- TECHNOLOGY, INC.) was used instead of the primary antibody. After immersing in PBS for 5 minutes twice, the secondary antibody, Anti-IgG, rabbit, goat-poly, Bio- tin (Vector Laboratories, Burlingame, CA, USA), was dripped on the sections (1:200) and left standing at room temperature for 30 minutes. After immersing in PBS for 5 minutes twice, vectastain ABC (Vector Laboratories, Burlingame, CA, USA) was dripped on the sections and left standing at room temperature for 30 minutes (ABC reaction). After immersing in PBS for 5 minutes twice, the sections were reacted with substrate DAB, and immersed in Milli-Q water. For counter staining, hematoxylin was used. The sections were then dehydrated and sealed.

The organs were similarly collected from 6-week-old

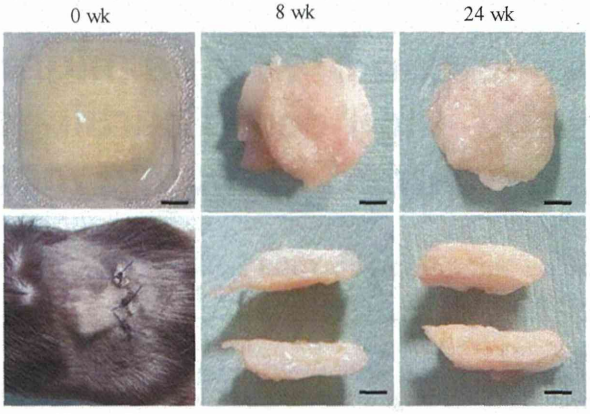

Figure 1. Macroscopic findings of tissue-engineered cartlage. Tisue-engineered cartilage comprised of PLLA scaffold with the mixture of green mouse auricular chondrocytes and atelocollagen was prepared (left top) subcutaneously transplanted into the dorsal region of C57BL/6 mice (left bottom). Whole (top) and half cross-section (bottom) of the transplants, 8 and 24 weeks after transplantation. Scale bar: 1 mm.

EGFP-transgenic mice (positive control) and 57BL/6 mice (negative control) and subjected to immunostaining of EGFP. The organ was judged as EGFP-positive when an EGFP-positive cell was present in one or more of the 10 sections [9].

3. RESULTS

The tissue-engineered cartilage removed 8 and 24 weeks after transplantation consisted in elastic soft tissue (**Figure 1, 8 and 24 wks**). The excised transplants were evaluated histologically and immunohistochemically. In toluidine blue staining, metachromasia was noted throughout the transplants at 8 and 24 weeks, suggesting the maturation of regenerative cartilage.

A large area in the transplants was occupied by regenerative cartilage at both 8 and 24 weeks, while the rate was almost similar between them (**Figures 2 (a)** and **(b)**). Under 490-nm excitation fluorescence, green fluorescence was noted in the cartilaginous region (**Figure 2**(c)). In immunohistochemical staining of EGFP, EGFP-positive cells were corresponding to chondrocytes in the cartilaginous region (**Figure 2**(d)). These findings suggested that chondrocytes in the regenerative cartilage were derived from the cells of the transplants.

The eight target organs were also excised when the transplant was removed at 8 or 24 weeks, and subjected to immunohistochemical staining of EGFP. In theEGFP-transgenic mice, EGFP-positive cells were present in all these organs (**Figures 3** and **4**, **EGFP**). In the C57BL/6 mice, no positive cells were noted in any of the eight organs (**Figures 3** and **4**, **before transplantation**). At 8 and 24 weeks after transplantation, no EGFP-positive cells were noted in any of the eight organs (**Figures 3** and **4**, **8 and 4 wks**).

The number of positive cells was 0 in any of the eight organs at 8 or 24 weeks after transplantation, showing that chondrocytes in the transplants did not migrate to other organs (**Table 1**).

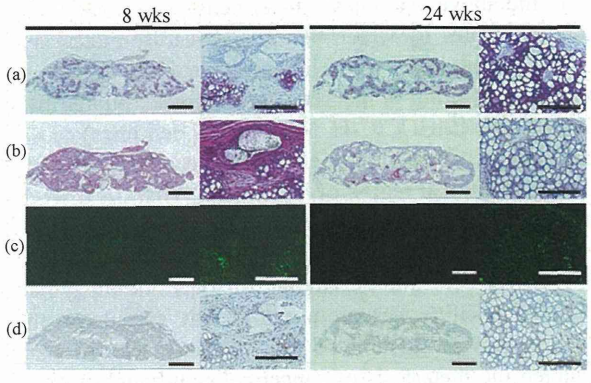

Figure 2. Histological analyses of tissue-engineered cartilage. (a) Toluidine blue staining of tissue-engineered cartilage. Abundant metachromasia was noted 8 and 24 weeks after transplantation, while cartilaginous tissue was extensively observed. (b) Hematoxylin and eosin staining of tissue-engineered cartilage, 8 and 24 weeks after transplantation. Maturation of tissue-engineered cartilage was observed at both weeks. (c) Localization of EGFP-positive chondrocytes was detected under 490-nm excitation fluorescence. (d) Immunohisto- chemical staining of EGFP in tissue-engineered cartilage. The cartilagenous region was constructed only with EGFP-positive transplanted chondrocytes, being consistent with the localization of EGFP-positive cells in C. Scale bar: 1 mm (low magnification) and 100 μm (high magnification).

4. DISCUSSION

We transplanted tissue-engineered cartilage containing EGFP-positive auricular chondrocytes into mice, and histologically confirmed that no chondrocytes migrated to the other organs 8 and 24 weeks after transplantation. As a phenomenon of cell migration between organs, me-

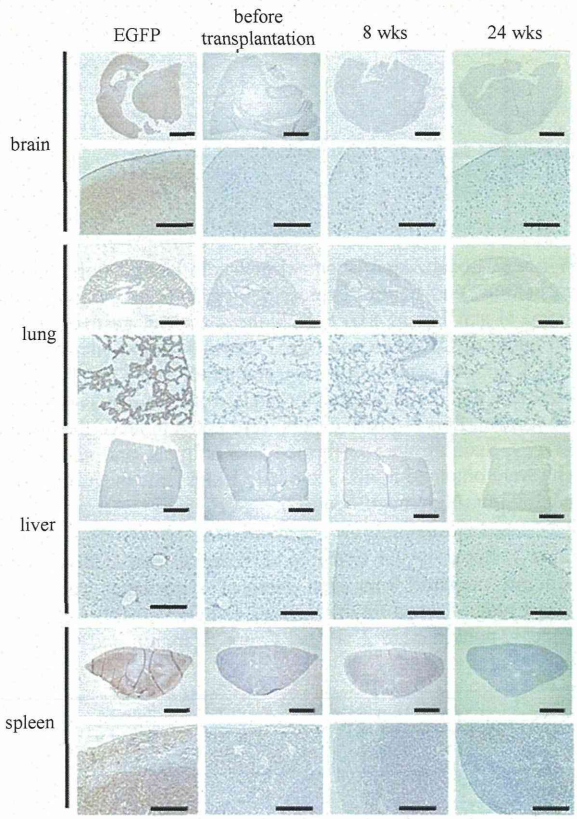

Figure 3. Localization of transplanted chondrocytes in cerebrum, lung, liver, and spleen. Typical photographs of immunohistochemical staining of EGFP in cerebrum, lung, liver, and spleen of C57BL/6 mice were shown before transplantation or at 8 and 24 weeks after transplantation. No EGFP-positive cells were noted in any of the organs. In green mice as the positive control, EGFP-positive cells were noted in all of the organs (EGFP). Staining was performed in 3 animals, and similar results were obtained in all. Scale bar: 1 mm (low magnification) and 100 μm (high magnification).

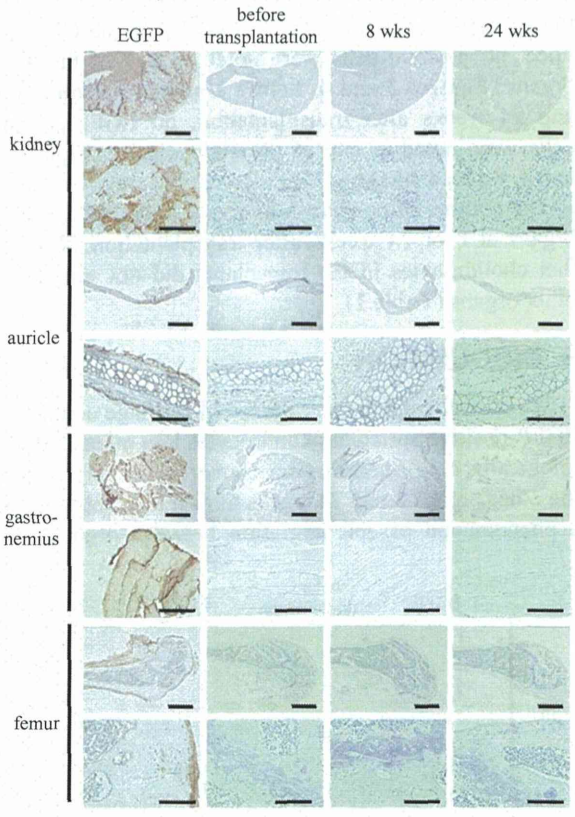

Figure 4. Localization of chondrocytes in kidney, auricle, gastrocnemius, and femur. Typical photographs of immunohistochemical staining of EGFP in kidney, auricle, gastrocnemius, and femur of C57BL/6 mice were shown before transplantation or at 8 and 24 weeks after transplantation. No EGFP-positive cells were noted in any of the organs. In green mice as the positive control, EGFP-positive cells were noted in all of the organs (EGFP). Staining was performed in 3 animals, and similar results were obtained in all. Scale bar: 1 mm (low magnification) and 100 μm (high magnification).

Table 1. Positivity for EGFP in each organ. Ten sections were randomly prepared from each organ of transplanted mice (n = 3), and judged based on the number of EGFP-positive cells as: Grade 1, none; Grade 2, a few; Grade 3, many; and Grade 4, all.

	8 wks			24 wks		
	No.1	No.2	No.3	No.1	No.2	No.3
brain	1	1	1	1	1	1
lung	1	1	1	1	1	1
liver	1	1	1	1	1	1
spleen	1	1	1	1	1	1
kidney	1	1	1	1	1	1
ear flap	1	1	1	1	1	1
muscle	1	1	1	1	1	1
bone	1	1	1	1	1	1

tastasis of cancer is generally known. Metastasis is defined as the spread of cancer cells from the original organ to another one [10]. Various models for metastasis of cancer cells after transplantation have been reported, and cancer metastasis is assumed to be induced by complex interactions of adhesion molecules [11], proteolytic enzymes [12], growth factors [13], vascularization [14], and chemokines [15], as a molecular mechanism.

For example, when U14 squamous cell carcinoma cells were intraperitoneally injected into ICR mice, cervical lymph node metastasis was noted after 15 - 20 days in 53% of the animals [16]. It has been speculated that lymph node metastasis starts with cancer cell infiltration in the sinus in the marginal region, and then cancer cells invaded the cortex and medulla, destroying the lymph node. One of molecules playing an important role in this tumor formation and metastasis was a matrix metalloproteinase (MMP). The MMPs degrades all types of extracellular matrix. The degradation of extracellular matrix was closely involved in metastasis of tumor cells. Among the MMP family, MMP-2 and -9 were considered to be particularly important factors for metastasis.

As another metastasis model, human lung cancer cells (MDA-MB-231 cells) have been known. When those cells were injected into the left ventricle of nude mice, bone metastasis was noted in 51.8% after 5 weeks [17]. In that model, many local and growth factors may be secreted from lung cancer cells, secondarily promoting the action of osteoclasts and advancing bone metastasis.

In the above examples, cancer cells were transplanted through routes by which they could readily metastasize to remote organs, such as intraperitoneal and cardiac injections, resulting in metastasis. In contrast, human liver cancer cells (MHCC97-H, MHCC97–L cell lines) caused lung metastasis even through subcutaneous trans- plantation in the dorsal region of nude mice. After 5 - 6 weeks of subcutaneous transplantation, 38% - 58% of recipient mice showed lung metastasis [18]. As characteristics of this cancer cell, a large amount of transforming growth factor β (TGFβ) was produced. It was speculated that such excess production of growth factor exceptionally enabled the metastasis of cancer cells, although it rarely occurs in subcutaneous transplantation models.

The cultured chondrocytes we investigated are also capable of producing MMPs [19] or growth factors, such including FGFs and TGF surperfamily [20]. However, the cultured chondrocytes conserve the function that they arrest the cell cycle in response to the stimulation for differentiation [21]. Moreover, we applied subcutaneous transplantation that hardly causes metastasis as the transplantation method. Thus, the cultured chondrocytes in this tissue-engineered cartilage may not cause the migration of cells to other organs.

We also used collagen hydrogel in order to prevent

leakage of transplanted cells from the scaffold. Generally, tumorigenicity becomes of concern in tissue engineering, if embryonic stem cells or induced pluripotent stem cells are used as cell sources [22]. These kinds of stem cells express adhesion molecules, such as E-cadherin. These molecules are considered to maintain the stem cell properties by forming aggregates [23]. However, in our tissue-engineered cartilage, the cultured chondrocytes were dispersed and mixed with collagen hydrogel, which may inhibit cadherin-mediated cell adhesion and enhanced matrix signals through integrins, promoting the differenttiation [24].

It has been reported that bone marrow-derived mesenchymal stem cells engrafted in other organs, such as cardiac muscle, when the cells were mobilized into the circulation [25]. As the mesenchymal stem cells are origin of chondrocytes, we should discuss the possibility of a similar phenomenon for the cultured chondrocytes. However, the mesenchymal stem cells have very high adhesive ability [26], and are as specific as they fuse with other kind of cells to exhibit pluripotency [27]. As the cultured chondrocytes do not have such prominent adhesiveness, there may be very little possibility that cultured chondrocytes engraft in other organs.

We had prepared the tissue-engineered cartilage using human auricular chondrocytes and clinically applied it for treatment of nasal deformation in cleft lip and palate patients [3]. The risk of migration of transplanted chondrocytes to distant organs should be seriously evaluated, even though there is very little possibility. In this study, no EGFP-positive cells were noted in any of the organs examined, supporting that subcutaneously-transplanted chondrocytes do not migrate to other organs through the circulation. In order to further develop regenerative medicine with cartilage prepared by tissue engineering, we should continue to consider the safety and efficacy of the tissue-engineered constructs from a variety of perspectives.

5. ACKNOWLEDGEMENTS

This work was supported by Grants-in-Aid for Scientific Research from the Ministry of Education, Culture, Sports, Science and Technology of Japan (MEXT, No. 24390451, and 25670847) and from the Ministry of Health, Labour and Welfare of Japan (MHLW, No. H24-Saisei-Ippan-005).

REFERENCES

[1] Brittberg, M., Lindahl, A., Nilsson A., Ohlsson, C., Isaksson, O. and Peterson, L. (1994) Treatment of deep cartilage defects in the knee with autologous chondrocyte transplantation. *The New England Journal of Medicine*, **331**, 889-895. http://dx.doi.org/10.1056/NEJM199410063311401

[2] Ochi, M., Uchio, Y., Kawasaki, K., Wakitani, S. and Iwasa, J. (2002) Transplantation of cartilage-like tissue made by tissue engineering in the treatment of cartilage defects of the knee. *Journal of Bone & Joint Surgery*, **84**, 571-578. http://dx.doi.org/10.1302/0301-620X.84B4.11947

[3] Hoshi, K., Fujihara, Y., Asawa, Y., Nishizawa, S., Kanazawa, S., Sakamoto, T., Watanabe, M., Ogasawara, T., Saijo, H., Mori, Y. and Takato, T. (2013) Recent trends of cartilage regenerative medicine and its application to the oral and maxillofacial surgery. *Oral Science International*, **15**, 15-19.

[4] Yamaoka, H., Tanaka, Y., Nishizawa, S., Asawa, Y., Takato, T. and Hoshi, K. (2010) The application of atelocollagen gel in combination with porous scaffolds for cartilage tissue engineering and its suitable condtions. *Journal of Biomedical Materials Research Part A*, **93**, 123-132. http://dx.doi.org/10.1002/jbm.a.32509

[5] Abedin, M., Tintut, Y. and Demer, L.L. (2004) Mesenchymal stem cells and the artery wall. *Circulation Research*, **95**, 671-676. http://dx.doi.org/10.1161/01.RES.0000143421.27684.12

[6] Asawa, Y., Sakamoto, T., Komura, M., Watanabe, M., Nishizawa, S., Takazawa, Y., Takato, T. and Hoshi, K. (2012) Early stage foreign body reaction against biodegradable polymer scaffolds affects tissue regeneration during the autologous transplantation of tissue-engineered cartilage in the canine model. *Cell Transplant*, **21**, 1431-1442. http://dx.doi.org/10.3727/096368912X640574

[7] Fujihara, Y., Takato, T. and Hoshi, K. (2010) Immunological response to tissue-engineered cartilage derived from auricular chondrocytes and a PLLA scaffold in transgenic mice. *Biomaterials*, **31**, 1227-1234. http://dx.doi.org/10.1016/j.biomaterials.2009.10.053

[8] Takahashi, T., Ogasawara, T., Kishimoto, J., Liu, G., Asato, H., Nakatsuka, T., Uchinuma, E., Nakamura, K., Kawaguchi, H., Chung, U.I., Takato, T. and Hoshi, K. (2005) Synergistic effects of FGF-2 with insulin or IGF-I on the proliferation of human auricular chondrocytes. *Cell Transplant*, **14**, 683-693. http://dx.doi.org/10.3727/000000005783982675

[9] Holleran, J.L., Miller, C.J., Edgehouse, N.L., Pretlow, T.P. and Culp, L.A. (2002) Differential experimental micrometastasis to lung, liver, and bone with lacZ-tagged CWR22R prostate carcinoma cells. *Clinical & Experimental Metastasis*, **19**, 17-24. http://dx.doi.org/10.1023/A:1013833111207

[10] Nguyen, D.X., Bos, P.D. and Massagué, J. (2009) Metastasis: From dissemination to organ-specific colonization. *Nature Reviews Cancer*, **9**, 274-284. http://dx.doi.org/10.1038/nrc2622

[11] Gao, J.L., Ji, X., He, T.C., Zhang, Q., He, K., Zhao, Y., Chen, S.H. and Lv, G.Y. (2013) Tetrandrine Suppresses Cancer Angiogenesis and Metastasis in 4T1 Tumor Bearing Mice. *Evidence-Based Complementary and Alternative Medicine*, **2013**, 265061. http://dx.doi.org/10.1155/2013/265061

[12] Matsumoto, Y., Zhang, Q., Akita, K., Nakada, H., Hamamura, K., Tsuchida, A., Okajima, T., Furukawa, K., Urano, T. and Furukawa, K. (2013) Trimeric Tn antigen on Syndecan-1 produced by ppGalNAc-T13 enhances

cancer metastasis via a complex formation with integrin α5β1 and matrix metalloproteinase 9. *Journal of Biological Chemistry*, **288**, 24264-24276. http://dx.doi.org/10.1074/jbc.M113.455006

[13] Chien, M.H., Lee, L.M., Hsiao, M., Wei, L.H., Chen, C,H., Lai, T.C., Hua, K.T., Chen, M.W., Sun, C.M. and Kuo, M.L. (2013) Inhibition of metastatic potential in breast carcinoma *in vivo* and *in vitro* through targeting VEGFRs and FGFRs. *Evidence-Based Complementary and Alternative Medicine*, **2013**, 718380. http://dx.doi.org/10.1155/2013/718380

[14] Huang, Q.B., Ma, X., Zhang, X., Liu, S.W., Ai, Q., Shi, T.P., Zhang, Y., Gao, Y., Fan, Y., Ni, D., Wang, B.J., Li, H.Z. and Zheng, T. (2013) Down-regulated miR-30a in clear cell renal cell carcinoma correlated with tumor hematogenous metastasis by targeting angiogenesis-specific DLL4. *PLoS One*, **8**, e67294. http://dx.doi.org/10.1371/journal.pone.0067294

[15] Yoshimura, T., Howard, O.M., Ito, T., Kuwabara, M., Matsukawa, A., Chen, K., Liu, Y., Liu, M., Oppenheim, J.J. and Wang, J.M. (2013) Monocyte chemoattractant protein-1/CCL2 produced by stromal cells promotes lung metastasis of 4T1 murine breast cancer cells. *PLoS One*, **8**, e58791. http://dx.doi.org/10.1371/journal.pone.0058791

[16] Zhao, X., Pang, L., Qian, Y., Wang, Q., Li, Y., Wu, M., Ouyang, Z., Gao, Z. and Qiu, L. (2013) An animal model of buccal mucosa cancer and cervical lymph node metastasis induced by U14 squamous cell carcinoma cells. *Experimental and Therapeutic Medicine*, **5**, 1083-1088. http://dx.doi.org/10.3892/etm.2013.938

[17] Jeong, J., Lee, K.S., Choi, Y.K., Oh, Y.J. and Lee, H.D. (2011) Preventive effects of zoledronic acid on bone metastasis in mice injected with human breast cancer cells. *Journal of Korean Medical Science*, **26**, 1569-1575. http://dx.doi.org/10.3346/jkms.2011.26.12.1569

[18] Li, G.C., Ye, Q.H., Dong, Q.Z., Ren, N., Jia, H.L. and Qin, L.X. (2012) TGF beta1 and related-Smads contribute to pulmonary metastasis of hepatocellular carcinoma in mice model. *Journal of Experimental & Clinical Cancer Research*, **14**, 93. http://dx.doi.org/10.1186/1756-9966-31-93

[19] Asawa, Y., Ogasawara, T., Takahashi, T., Yamaoka, H., Nishizawa, S., Matsudaira, K., Mori, Y., Takato, T. and Hoshi, K. (2009) Aptitude of auricular and nasoseptal chondrocytes cultured under a monolayer or three-dimensional condition for cartilage tissue engineering. *Tissue Engineering Part A*, **15**, 1109-1118. http://dx.doi.org/10.1089/ten.tea.2007.0218

[20] Yamaoka, H., Nishizawa, S., Asawa, Y., Fujihara, Y., Ogasawara, T., Yamaoka, K., Nagata, S., Takato, T. and Hoshi, K. (2010) Involvement of fibroblast growth factor 18 in dedifferentiation of cultured human chondrocytes. *Cell Proliferation*, **43**, 67-76. http://dx.doi.org/10.1111/j.1365-2184.2009.00655.x

[21] Liu, G., Kawaguchi, H., Ogasawara, T., Asawa, Y., Kishimoto, J., Takahashi, T., Chung, U.I., Yamaoka, H., Asato, H., Naka-mura, K., Takato, T. and Hoshi, K. (2007) Optimal combination of soluble factors for tissue engineering of permanent cartilage from cultured human chondrocytes. *Journal of Biological Chemistry*, **282**, 20407-20415. http://dx.doi.org/10.1074/jbc.M608383200

[22] Menendez, S., Camus, S., Herreria, A., Paramonov, I., Morera, L.B., Collado, M., Pekarik, V., Maceda, I., Edel, M., Consiglio, A., Sanchez, A., Li, H., Serrano, M. and Belmonte, J.C. (2012) Increased dosage of tumor suppressors limits the tumorigenicity of iPS cells without affecting their pluripotency. *Aging Cell*, **11**, 41-50. http://dx.doi.org/10.1111/j.1474-9726.2011.00754.x

[23] Chen, T., Yuan, D., Wei, B., Jiang, J., Kang, J., Ling, K., Gu, Y., Li, J., Xiao, L. and Pei. G. (2010) E-cadherin-mediated cell-cell contact is critical for induced pluripotent stem cell generation. *Stem Cells*, **28**, 1315-1325. http://dx.doi.org/10.1002/stem.456

[24] Yamaoka, H., Asato, H., Ogasawara, T., Nishizawa, S., Takahashi, T., Nakatsuka, T., Koshima, I., Nakamura, K., Kawaguchi, H., Chung, U.I., Takato, T. and Hoshi, K. (2006) Cartilage tissue engineering using human auricular chondrocytes embedded in different hydrogel materials. *Journal of Biomedical Materials Research Part A*, **78**, 1-11. http://dx.doi.org/10.1002/jbm.a.30655

[25] Barbash, I.M., Chouraqui, P., Baron, J., Feinberg, M.S., Etzion, S., Tessone, A., Miller, L., Guetta, E., Zipori, D., Kedes, L.H., Kloner, R.A. and Leor, J. (2003) Systemic delivery of bone marrow-derived mesenchymal stem cells to the infarcted myocardium: feasibility, cell migration, and body distribution. *Circulation*, **108**, 863-868. http://dx.doi.org/10.1161/01.CIR.0000084828.50310.6A

[26] Liu, G., Iwata, K., Ogasawara, T., Watanabe, J., Fukazawa, K., Ishihara, K., Asawa Y., Fujihara, Y., Chung, U.L., Moro, T., Takatori, Y., Takato, T., Nakamura, K., Kawaguchi, H. and Hoshi, K. (2010) Selection of highly osteogenic and chondrogenic cells from bone marrow stromal cells in biocompatible polymer-coated plates. *Journal of Biomedical Materials Research Part A*, **92**, 1273-1282. http://dx.doi.org/10.1002/jbm.a.32460

[27] Terada, N., Hamazaki, T., Oka, M., Hoki, M., Mastalerz, D.M., Nakano, Y., Meyer, E.M., Morel, L., Petersen, B.E. and Scott, E.W. (2002) Bone marrow cells adopt the phenotype of other cells by spontaneous cell fusion. *Nature*, **416**, 542-545. http://dx.doi.org/10.1038/nature730

